Magnetic Flux Signal Simulation with 16-channel Sensor Array to Specify Accurate IGBT Current Distribution

Magnetic flux signal simulation with 16-channel sensor array to specify accurate IGBT current distribution

M. Tsukuda[a,b], K. Matsuo[c], H. Tomonaga[b] , S. Okoda[d], R. Noda[c], K. Tashiro[e] and I. Omura[b]

[a] City of Kitakyushu, 1-8 Hibikino, Wakamatsu-ku, Kitakyushu, Japan
[b] Kyushu Institute of Technology, 1-1 Sensui-cho, Tobata-ku, Kitakyushu, Japan
[c] C.D.N. CORPORATION, 1-18-22 Ohtsubo-higashi, Miyazaki, Japan
[d] COPER ELECTRONICS LTD., 43 Funako, Atsugi, Japan
[e] HOH KOH SYA Co., Ltd., 2-7-30 Kamiitouzu, Kokurakita-ku, Kitakyushyu, Japan

Summary

Current crowding of IGBT and power diodes in a chip or among chips is a barrier to the realization of highly-reliable power modules and power electronics systems. Current crowding occurs because of stray inductance imbalance, difference of chip characteristics and temperature imbalance among chips. Although current crowding among IGBT or power diode chips has been analyzed by numerical simulation, no sensor with sufficiently high special resolution and fast measurement time has yet been developed. Therefore, we developed a 16-channel sensor array and demonstrated IGBT current distribution imaging. By using the developed simulation method for the sensor array, the accuracy of the magnetic flux signals was confirmed. In future work, we will apply the simulation method to specify the IGBT current distribution corresponding to the structure of bonding wire and other wiring.

1 Introduction

Current crowding of IGBT and power diodes in a chip or among chips is a barrier to the realization of highly-reliable power electronics systems. Current crowding occurs because of the stray inductance [1], difference of chip characteristics or temperature imbalance among chips [2, 3]. Although current crowding among IGBT or power diode chips has been analyzed by numerical simulations [4, 5], no sensor with sufficiently high special resolution and fast measurement time has yet been developed. For example, the commercialized current transformer (CT) and Rogowski coil is too large to realize the high special resolution around bonding wires [6-8].

The 16-channel sensor array makes it possible to imagine the current distribution of IGBT chips by acquiring a local magnetic flux over bonding wires without the insertion of a sensor [9 – 14] (see Figure 1). Fast measurement time and high special resolution are realized without making any change to the chip wiring. By applying the developed simulation method for the sensor array, the accuracy of the magnetic flux signals was confirmed.

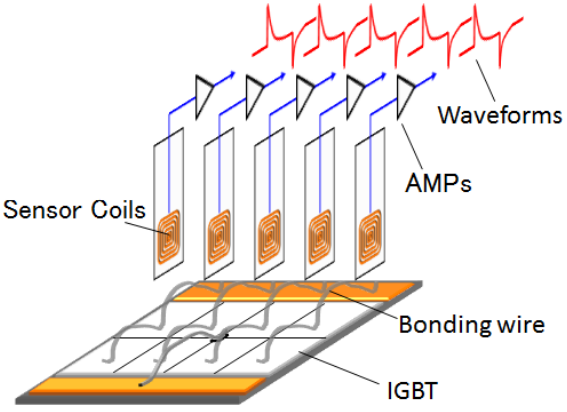

Fig. 1. Schematic view of measurement method of magnetic flux signals.

2 Current distribution imaging of IGBT from magnetic flux signal with 16-channel sensor array

The 16-channel sensor array consists of film sensors, analog amps and a shield case (see Figure 2). Regarding the sensors, the side of the spiral coil on polyimide film is 1 mm x 1 mm and 5 turns each on both sides. The sensitivity is about 100 mV/A after amplifying in this experiment. And the 16 sensors are laminated with a position error of plus or minus 20 μm. A 16-channel sensor array is installed near the IGBT chips

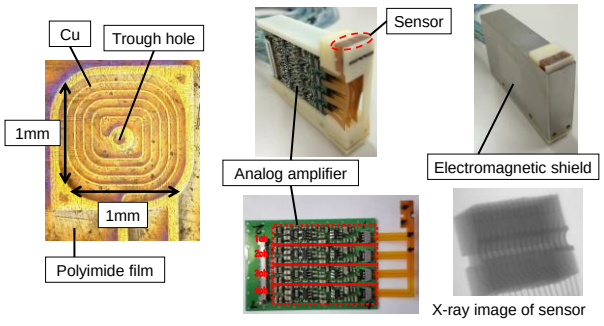

Fig. 2. Sensor coil structure and 16-channel sensor array configuration.

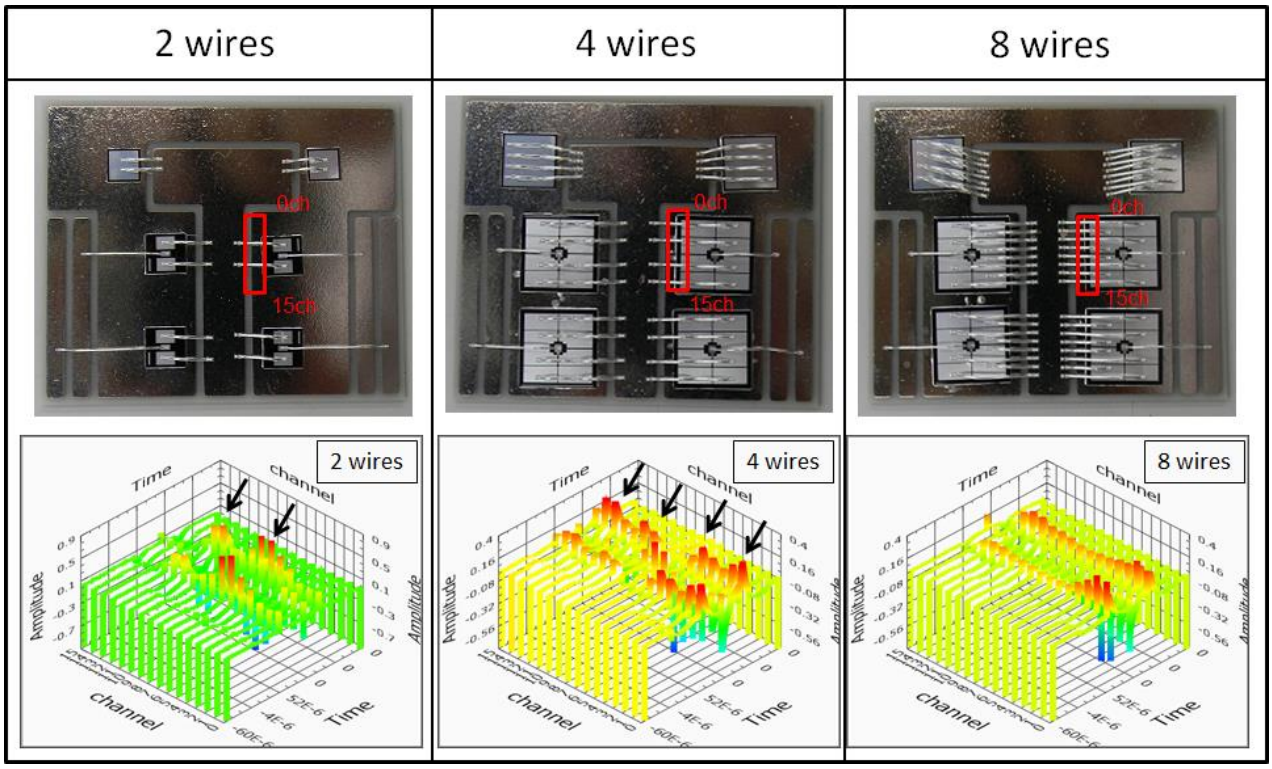

Fig. 3. Demonstration of current distribution imaging with 2, 4 and 8 bonding wires.

and bonding wires. However, the sensor array detects noise from untargeted wiring. Therefore, noise reduction is required. The analog amps near the sensor array increase the signal to noise ratio and the shield case reduces the effect of direct noise on the amp circuit boards.

It is difficult to realise flat sensitivity of the sensor array because of the non-uniformity of the resistor and capacitor for analog amps and error of the sensor array levelness. However, solving the problem by hardware architecture is time-consuming and expensive to maintain flat sensitivity. Therefore, we propose performing digital calibration with correction values by software (LabVIEW program). The digital calibration is carried out according to the following procedures. Firstly, one wire flowing pulse current is scanned under the 16-channel sensor array and the maximum signal existing just under each sensor is selected to calibrate the non-uniformity of the sensitivity. Secondly, the correction values for agreement with all signal waveforms are extracted. Finally, the original signal waveform is calibrated with the correction values by the LabVIEW program. The digital calibration is demonstrated. The sensitivity error in space is successfully reduced by the digital calibration and the sensitivity is to be flat. In addition, the signal waveforms also perfectly agree.

The noise shield effect is confirmed by signal waveform from amps with/without the shield case. The input terminals of the amps are short circuited in the experiment. Thus, the signal waveforms directly show the noise effect in nearby wiring. It is confirmed that the noise effect is greatly reduced to 10% with the shield case.

To cancel the effect of noise from other current path to sensor coil, a differential signal of low position to high position from target bonding wires is employed for current distribution imaging because the magnetic flux from distant current is considered almost the same regardless of height. On the other hand, the magnetic flux from nearby bonding wires differs corresponding to the height.

The current distribution imaging is demonstrated by the differential signal for the IGBT chip with 2, 4 and 8 bonding wires with the 16-channnel micro magnetic flux sensor array. The switching condition is inductive load and double pulses. The DC voltage and turn-off current are 100 V and 100 A, respectively. The signal distribution of 2 and 4 bonding wires successfully

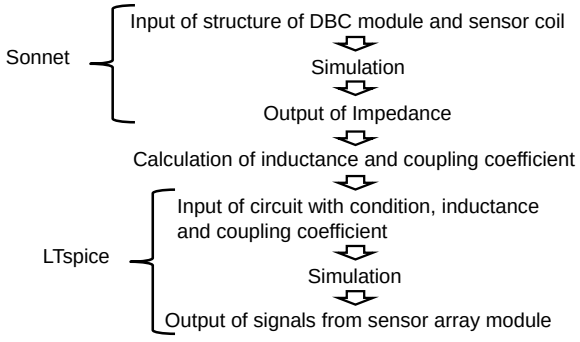

Fig. 4. Workflow of magnetic signal simulation.

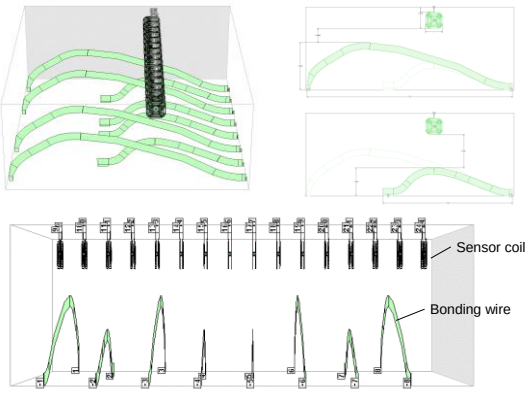

Fig. 5. Input data of bonding wires and sensor coils for simulation with Sonnet software.

reflects the current path (see Figure 3). For the 8 bonding wires, the signals are continuous because the space between each bonding wire is very small. In addition, the signal distribution has several features. The signals at both outsides and center are comparatively low.

3 Magnetic flux signal simulation method with inductance and coupling coefficient

We simulated a magnetic signal by the following workflow (see Figure 4). Firstly, we input the structure of the bonding wires and the coils by Sonnet software (see Figure 5) and output impedance values to calculate inductances and coupling coefficients. Using a simple two-dimensional model greatly shortened the analysis time. Secondly, the inductances and coupling coefficients of all combinations between bonding wires and sensor coils were calculated by Microsoft Excel from the impedance (see Figure 6). The impedance is represented at 100 MHz based on the switching speed. The coupling coefficients between the sensor coils are only about ten times larger than the coupling coefficients between the sensor coils and bonding wires. Therefore, the proximity effect is expected to be negligibly small because the current flow of the bonding wire is several orders of magnitude greater. Finally, the waveform of the magnetic flux signal is calculated from the circuit with the inductance and the coupling coefficients by LTspice (see Figure 7). The described workflow allows quick simulation. The magnetic flux simulation successfully shows the same features as the experimental results (see Figure 8). It is assumed that the current equally flows in every wire. Saturation of an amplifier is also simulated faithfully.

4 Conclusion

We developed a magnetic flux signal simulation method for the sensor array. By using this method, experimental magnetic flux signals were simulated and confirmed. In future, we will apply the simulation method to try to specify the current distribution corresponding to the structure of bonding wire and other wiring.

5 Acknowledgment

This study was supported by the Strategic Key Technology Advancement Support Project (Acceptance No.: 24194003018) of the Ministry of Economy, Trade and Industry.

Bonding wires

Sensor coils

		Bonding wire 1	Bonding wire 2	Bonding wire 3	Bonding wire 4	Bonding wire 5	Bonding wire 6	Bonding wire 7	Bonding wire 8	Sensor coil 01	Sensor coil 02	Sensor coil 03	Sensor coil 04	Sensor coil 05	Sensor coil 06	Sensor coil 07	Sensor coil 08	Sensor coil 09	Sensor coil 10	Sensor coil 11	Sensor coil 12	Sensor coil 13	Sensor coil 14	Sensor coil 15	Sensor coil 16
		L1	L2	L3	L4	L5	L6	L7	L8	L9	L10	L11	L12	L13	L14	L15	L16	L17	L18	L19	L20	L21	L22	L23	L24
Bonding wire 1	L1	1.000000	0.068908	0.046085	0.006228	0.001883	0.002714	0.000057	0.000463	0.008470	0.009142	0.006895	0.004500	0.002775	0.001677	0.001011	0.000614	0.000379	0.000239	0.000154	0.000102	0.000069	0.000046	0.000030	0.000017
Bonding wire 2	L2	0.068908	1.000000	0.080611	0.034375	0.011681	0.002069	0.001885	0.000029	0.004150	0.006885	0.008098	0.007115	0.004988	0.003012	0.001638	0.000807	0.000345	0.000105	0.000010	0.000057	0.000069	0.000063	0.000049	0.000031
Bonding wire 3	L3	0.046085	0.080611	1.000000	0.081626	0.023742	0.022944	0.002040	0.003414	0.002756	0.005556	0.009278	0.013308	0.015170	0.013074	0.009209	0.005889	0.003627	0.002211	0.001352	0.000836	0.000522	0.000326	0.000198	0.000106
Bonding wire 4	L4	0.006228	0.034375	0.081626	1.000000	0.126639	0.023697	0.012084	0.002088	0.000419	0.000922	0.001794	0.003223	0.005252	0.007360	0.008233	0.007086	0.004895	0.002911	0.001553	0.000749	0.000313	0.000098	0.000007	0.000019
Bonding wire 5	L5	0.001883	0.011681	0.023742	0.126639	1.000000	0.081561	0.033262	0.007188	0.000069	0.000174	0.000408	0.000875	0.001731	0.003158	0.005194	0.007319	0.008217	0.007084	0.004922	0.002948	0.001596	0.000794	0.000358	0.000135
Bonding wire 6	L6	0.002714	0.002069	0.022944	0.023697	0.081561	1.000000	0.081525	0.055806	0.000135	0.000282	0.000497	0.000834	0.001384	0.002298	0.003804	0.006199	0.009665	0.013528	0.015272	0.013083	0.009129	0.005700	0.003287	0.001642
Bonding wire 7	L7	0.000057	0.001885	0.002040	0.012084	0.033262	0.081525	1.000000	0.078803	0.000026	0.000045	0.000056	0.000047	0.000001	0.000122	0.000378	0.000873	0.001761	0.003218	0.005277	0.007407	0.008282	0.007089	0.004763	0.002482
Bonding wire 8	L8	0.000463	0.000029	0.003414	0.002088	0.007188	0.055806	0.078803	1.000000	0.000023	0.000048	0.000079	0.000124	0.000191	0.000299	0.000476	0.000773	0.001274	0.002117	0.003516	0.005740	0.008913	0.012244	0.013000	0.009086
Sensor coil 01	L9	0.008470	0.004150	0.002756	0.000419	0.000069	0.000135	0.000026	0.000023	1.000000	0.058796	0.011685	0.004143	0.001842	0.000918	0.000491	0.000276	0.000161	0.000097	0.000059	0.000037	0.000024	0.000015	0.000009	0.000005
Sensor coil 02	L10	0.009142	0.006885	0.005556	0.000922	0.000174	0.000282	0.000045	0.000048	0.058796	1.000000	0.060809	0.012699	0.004674	0.002135	0.001087	0.000592	0.000338	0.000200	0.000121	0.000075	0.000047	0.000030	0.000018	0.000009
Sensor coil 03	L11	0.006895	0.008098	0.009278	0.001794	0.000408	0.000497	0.000056	0.000079	0.011685	0.060809	1.000000	0.061311	0.012989	0.004842	0.002236	0.001149	0.000630	0.000362	0.000216	0.000131	0.000081	0.000050	0.000030	0.000016
Sensor coil 04	L12	0.004500	0.007115	0.013308	0.003223	0.000875	0.000834	0.000047	0.000124	0.004143	0.012699	0.061311	1.000000	0.061467	0.013087	0.004904	0.002275	0.001174	0.000647	0.000373	0.000222	0.000134	0.000082	0.000048	0.000025
Sensor coil 05	L13	0.002775	0.004988	0.015170	0.005252	0.001731	0.001384	0.000001	0.000191	0.001842	0.004674	0.012989	0.061467	1.000000	0.061525	0.013127	0.004929	0.002291	0.001184	0.000653	0.000376	0.000222	0.000132	0.000076	0.000039
Sensor coil 06	L14	0.001677	0.003012	0.013074	0.007360	0.003158	0.002298	0.000122	0.000299	0.000918	0.002135	0.004842	0.013087	0.061525	1.000000	0.061552	0.013144	0.004939	0.002297	0.001187	0.000653	0.000373	0.000217	0.000123	0.000061
Sensor coil 07	L15	0.001011	0.001638	0.009209	0.008233	0.005194	0.003804	0.000378	0.000476	0.000491	0.001087	0.002236	0.004904	0.013127	0.061552	1.000000	0.061562	0.013150	0.004942	0.002298	0.001184	0.000647	0.000364	0.000202	0.000099
Sensor coil 08	L16	0.000614	0.000807	0.005889	0.007086	0.007319	0.006199	0.000873	0.000773	0.000276	0.000592	0.001149	0.002275	0.004929	0.013144	0.061562	1.000000	0.061565	0.013150	0.004940	0.002292	0.001175	0.000632	0.000340	0.000164
Sensor coil 09	L17	0.000379	0.000345	0.003627	0.004895	0.008217	0.009665	0.001761	0.001274	0.000161	0.000338	0.000630	0.001174	0.002291	0.004939	0.013150	0.061565	1.000000	0.061562	0.013144	0.004930	0.002277	0.001151	0.000595	0.000279
Sensor coil 10	L18	0.000239	0.000105	0.002211	0.002911	0.007094	0.013528	0.003218	0.002117	0.000097	0.000200	0.000362	0.000647	0.001184	0.002297	0.004942	0.013150	0.061562	1.000000	0.061550	0.013127	0.004906	0.002239	0.001091	0.000495
Sensor coil 11	L19	0.000154	0.000010	0.001352	0.001553	0.004922	0.015272	0.005277	0.003516	0.000059	0.000121	0.000216	0.000373	0.000653	0.001187	0.002298	0.004940	0.013144	0.061550	1.000000	0.061528	0.013092	0.004846	0.002140	0.000922
Sensor coil 12	L20	0.000102	0.000057	0.000836	0.000749	0.002948	0.013083	0.007407	0.005740	0.000037	0.000075	0.000131	0.000222	0.000376	0.000653	0.001184	0.002292	0.004930	0.013127	0.061528	1.000000	0.061474	0.012994	0.004678	0.002140
Sensor coil 13	L21	0.000069	0.000069	0.000522	0.000313	0.001596	0.009129	0.008282	0.008913	0.000024	0.000047	0.000081	0.000134	0.000222	0.000373	0.000647	0.001175	0.002277	0.004906	0.013092	0.061474	1.000000	0.061315	0.012702	0.004846
Sensor coil 14	L22	0.000046	0.000063	0.000326	0.000098	0.000794	0.005700	0.007089	0.012244	0.000015	0.000030	0.000050	0.000082	0.000132	0.000217	0.000364	0.000632	0.001151	0.002239	0.004846	0.012994	0.061315	1.000000	0.060810	0.012994
Sensor coil 15	L23	0.000030	0.000049	0.000198	0.000007	0.000358	0.003287	0.004763	0.013000	0.000009	0.000018	0.000030	0.000048	0.000076	0.000123	0.000202	0.000340	0.000595	0.001091	0.002140	0.004678	0.012702	0.060810	1.000000	0.061474
Sensor coil 16	L24	0.000017	0.000031	0.000106	0.000019	0.000135	0.001642	0.002482	0.009086	0.000005	0.000009	0.000016	0.000025	0.000039	0.000061	0.000099	0.000164	0.000279	0.000495	0.000922	0.001846	0.004146	0.011687	0.058799	1.000000

Fig. 6. Input data of bonding wires and sensor coils for simulation with Sonnet software.

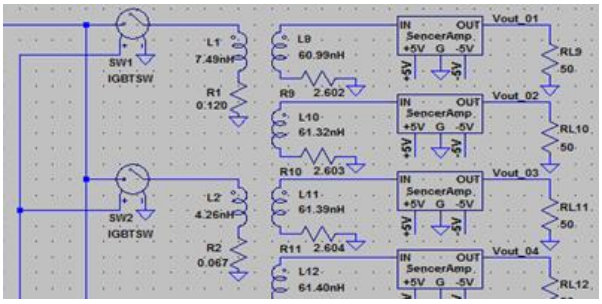

Fig. 7. A part of the circuit of LTspice simulation with coupling coefficients for calculation of magnetic flux signal waveforms.

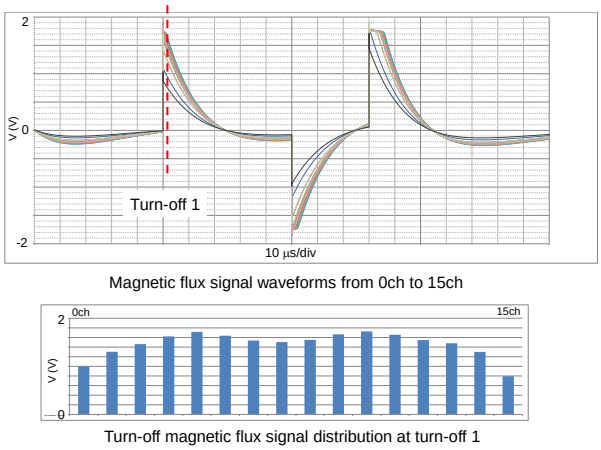

Fig. 8. Simulated magnetic flux signal distribution with the same current flow in every wire.

We would like to thank Nagayuki Shinohara at HOH KOH SYA Co., Ltd. for the design and fabrication of the 16-channel sensor array. We would also like to thank Kazunori Nagatomo at C.D.N. CORPORATION for the design and evaluation of analog amps.

6 References

[1] K. Xing, F.C. Lee, D. Boroyevich, “Extraction of parasitics within wire-bond IGBT modules,” Proc APEC '98, pp. 497‑503, 1988.

[2] M. Riccio, L. Rossi, A. Irace, E. Napoli, G. Breglio, P. Spirito, R. Tagami, Y. Mizuno, “Analysis of large area trench-IGBT current distribution under UIS test with the aid of lock-in thermography,” Microelectronics Reliability, Vol.50, pp. 1725‑1730, 2010.

[3] Yohei Iwahashi,Yoshihito Mizuno, Masafumi Hara, Ryuzo Tagami, Masanori Ishigaki, “Analysis of current distribution on IGBT under unclamped inductive,” Microelectronics Reliability, Vol.52, pp. 2430‑2433, 2012.

[4] T. Shoji, M. Ishiko, T. Fukami, T. Ueta, K. Hamada, “Investigations on current filamentation of IGBTs under unclamped inductive switching conditions,” Proc. of ISPSD'05, pp. 227‑230, 2005.

[5] S. Milady, D. Silber, F. Pfirsch, F.-J., “Niedernostheide, Simulation studies and modeling of short circuit current oscillations in IGBTs,” Proc ISPSD'09, pp. 37‑40, 2009.

[6] Pearson ELECTRONICS Wideband Current Monitors, http://www.pearsonelectronics. com/.

[7] D.A. Ward, J. Exon, T. La, “Using Rogowski coils for transient current measurements, ” Eng. Sci. Educ. J. 2, pp. 105‑113, 1993.

[8] W.F. Ray, C.R. Hewson, “High performance Rogowski current transducers,” Conference record of the 2000 IEEE, Vol. 5, pp. 3083‑3090, 2000.

[9] Yuya Kasho, Hidetoshi Hirai, Masanori Tsukuda, Ichiro Omura, “Tiny-scale ‘stealth’ current sensor to probe power semiconductor device failure,” Microelectronics Reliability, Vol. 51, pp. 1689‑1692, 2011.

[10] H. Hirai, Y. Kasho, M. Tsukuda, I. Omura, “Bonding wire current measurement with tiny filmcurrent sensors,” Proc. of ISPSD, pp. 287–290, 2012.

[11] H. Shiratsuchi, K. Matsushita, I. Omura, “IGBT chip current imaging system by scanning local magnetic field,” Microelectrononics Reliability, Vol. 53, pp. 1409–1412, 2013.

[12] Masanori Tsukuda, Seiichi Okoda, Ryuzo Noda, Katsuji Tashiro and Ichiro Omura, “High-throughput DBC-assembled IGBT screening for power module,” International Conference on Integrated Power Electronics Systems, 2014.

[13] H. Tomonaga, M. Tsukuda, S. Okoda, R. Noda, K. Tashiro and I. Omura, “16-Channel micro magnetic flux sensor array for IGBT current distribution measurement,” Microelectronics Reliability, 2015.

[14] M. Tsukuda, H. Tomonaga, S. Okoda, R. Noda, K. Tashiro and I. Omura, “High-throughput and full automatic DBC-module,” Microelectronics Reliability, 2015.